Cryptococcus neoformans evades pulmonary immunity by modulating xylose precursor transport

Lucy X. Li[a,*,+], Camaron R. Hole[a,+], Javier Rangel-Moreno[b], Shabaana A. Khader[a], and Tamara L. Doering[a,#]

[a]Department of Molecular Microbiology, Washington University School of Medicine, St. Louis, Missouri, USA

[b]Department of Medicine, Allergy/Immunology, and Rheumatology, University of Rochester School of Medicine, Rochester, New York, USA

Running Head: Xylose precursors and cryptococcal immunity

[#]Address correspondence to Tamara L. Doering, doering@wustl.edu.

*Present address: Department of Medicine, Johns Hopkins University School of Medicine, Baltimore, Maryland, USA

[+]Co-first authors

ABSTRACT

Cryptococcus neoformans is a fungal pathogen that kills almost 200,000 people each year and is distinguished by abundant and unique surface glycan structures that are rich in xylose. A mutant strain of *C. neoformans* that cannot transport xylose precursors into the secretory compartment is severely attenuated in virulence in mice, yet surprisingly is not cleared. We found that this strain failed to induce the non-protective T helper cell type 2 (Th2) responses characteristic of wild-type infection, instead promoting sustained Interleukin (IL)-12p40 induction and increased IL-17A (IL-17) production. It also stimulated dendritic cells to release high levels of pro-inflammatory cytokines, a behavior we linked to xylose expression. We further discovered that inducible bronchus associated lymphoid tissue (iBALT) forms in response to infection with either wild-type cryptococci or the mutant strain with reduced surface xylose; although iBALT formation is slowed in the latter case, the tissue is better organized. Finally, our temporal studies suggest that lymphoid structures in the lung restrict the spread of mutant fungi for at least 18 weeks after infection, in contrast to ineffective control of the pathogen after infection with wild-type cells. These studies demonstrate the role of xylose in modulation of host response to a fungal pathogen and show that cryptococcal infection triggers iBALT formation.

INTRODUCTION

Cryptococcus neoformans is a ubiquitous environmental fungus that causes pneumonia and meningitis. This opportunistic pathogen infects over a million individuals each year, with overall mortality exceeding 20% (1-3). Patient immune status is the main determinant of infection outcome, highlighting the importance of efficient host immune responses in the control of cryptococcosis.

C. neoformans infection begins when the organism is inhaled, which is followed by its proliferation in the lungs. This pulmonary infection may then disseminate to the brain, where it causes a frequently lethal meningoencephalitis. In the lungs, *C. neoformans* first interacts with host macrophages and dendritic cells (DC). These engulf the fungus and migrate to draining lymph nodes, where they present antigen to T cells to initiate the adaptive immune response. The protective immune response to this infection is primarily mediated by T cells: T helper cell type 1 (Th1) responses are protective against *C. neoformans* (4) and T helper type 17 (Th17) responses likely participate in pathogen clearance at mucosal surfaces (5-7). In contrast, T helper cell type 2 (Th2) responses are considered detrimental for protective immunity, leading to fungal growth and facilitating dissemination to the CNS (8, 9). The induction of these non-protective responses is not well understood, but cryptococcal glycans may contribute to this process (10).

Glycan structures participate in antigen recognition, immune activation, and immune regulation in multiple organisms (11). In *C. neoformans* the major virulence factor, a polysaccharide capsule, modulates the immune response via multiple mechanisms, including dampening immune cell activation and impeding phagocytosis (12, 13). The capsule is

41 primarily composed of two large polysaccharides: glucuronoxylomannan (GXM) and glu-
42 curonoxylomannogalactan (GXMGal) (14, 15). One major component of both polymers is
43 xylose (Xyl), which comprises almost one fourth of the polysaccharide capsule mass (16).
44 Xylose also occurs in cryptococcal glycolipids (17) and as both Xyl and Xyl-phosphate
45 modifications of protein-linked glycans (18-20). We demonstrate here that Xyl plays a
46 critical role in the immune recognition of, and response to, *C. neoformans.*

47 The incorporation of Xyl into cryptococcal glycan structures occurs in the lumen of the
48 secretory pathway, via enzymatic reactions that use the substrate molecule UDP-Xyl.
49 This xylose donor is imported into the synthetic compartment by two transporters, Uxt1
50 and Uxt2 (21). A mutant strain that lacks both transporters (*uxt1*Δ *uxt2*Δ) exhibits defects
51 in xylosylation, including incomplete synthesis of capsule polysaccharides, and consider-
52 able attenuation of virulence in mouse models of infection. Surprisingly, despite its com-
53 promised virulence, which contrasts with the rapid lethality of wild-type (WT) infection, the
54 mutant strain persists for months in the lungs of infected mice (21).

55 In pursuing the mechanism of *uxt1*Δ *uxt2*Δ persistence, we found that infection with the
56 mutant failed to induce the Th2 responses provoked by WT fungi, although it did promote
57 production of IL-12p40 and IL-17, likely via enhanced stimulation of DCs. The correspond-
58 ing inflammatory response was enriched in T and B cells, which were required for the
59 prolonged survival of the infected animals. Inflammation in the lung, although it increased
60 slowly compared to the response to WT infection, appeared to effectively contain the mu-
61 tant yeast cells for an extended period after infection. Finally, we observed the formation
62 of inducible bronchus associated lymphoid tissue (iBALT) in the lungs of both WT and
63 *uxt1*Δ *uxt2*Δ infected mice. iBALT resembles secondary lymphoid organs (lymph nodes)

64 in cellular composition and organization, with two distinctive zones: a central B cell follicle
65 and surrounding T cell zone (22). The T cell zone contains CD4 and CD8 T cells as well
66 as DCs (23); the B cell zone contains mainly follicular B cells and its organization is main-
67 tained by the continuous production of CXCL13 (24). DC activation and cytokine produc-
68 tion are also required for iBALT formation and maintenance (23, 25). In the lungs of mice
69 infected with the *uxt1*Δ *uxt2*Δ mutant, iBALT formation was significantly delayed. How-
70 ever, once formed, it was better organized than the iBALT produced when mice were
71 infected with fully xylosylated WT *C. neoformans.* Together, these results suggest that
72 luminal Xyl modifications of cryptococcal glycoconjugates alter immune recognition and
73 activation of immune cells, events that are required for efficient control of *C. neoformans*
74 infection.
75

76 **RESULTS**

77 *UDP-Xyl transport is required for cryptococcal virulence and dissemination*

78 We previously observed that a *C. neoformans* strain lacking UDP-Xyl transporters (*uxt1*Δ
79 *uxt2*Δ) was highly attenuated in virulence compared to the WT parental strain KN99α, yet
80 remained in the lungs of asymptomatic mice for at least 100 days after infection (21).
81 While defects in the mutant strain, such as altered capsule and a slightly decreased
82 growth rate, might explain its reduced virulence, this persistence was surprising. To in-
83 vestigate the development of this chronic infection, we first examined the kinetics of fungal
84 burden in mice after intranasal inoculation with WT and mutant strains. In A/JCr mice
85 infected intranasally with WT fungi, which typically succumb to infection roughly 18 days
86 post-infection (dpi), we observed a rapid and significant increase in pulmonary fungal

87 burden (Fig. 1A) along with significant dissemination to the spleen (Fig. 1B) and brain
88 (Fig. 1C). In contrast, the pulmonary burden in *uxt1*Δ *uxt2*Δ-infected mice increased
89 slowly from initial inoculum levels to a modest peak at 63 dpi (Fig. 1A). Colony-forming
90 units in the lung then gradually declined, although even after six months only 30% of mice
91 showed complete clearance (Fig. 1A, 189 dpi). Although *uxt1*Δ *uxt2*Δ infection was not
92 restricted to the lungs, only a fraction of the mice had measurable mutant cells in the
93 spleen (Fig. 1B) and brain (Fig. 1C) at 63 dpi. Furthermore, this limited dissemination
94 was only observed at the times of highest lung burden (63 and 126 dpi), with no fungi
95 detected at distal sites by 189 dpi (Fig. 1B, Fig. 1C).
96
97 *Cryptococcal xylosylation influences production of pulmonary cytokines and cellular im-*
98 *mune response*
99 We next sought to identify the mechanism(s) responsible for the unexpected persistence
100 of *uxt1*Δ *uxt2*Δ after intranasal infection. As summarized above, protection against *C.*
101 *neoformans* is generally associated with production of type 1 cytokines like interleukin
102 (IL)-2, IL-12, interferon gamma (IFN-γ), and tumor necrosis factor alpha (TNF-α). In con-
103 trast, a Th2 response to cryptococcal infection (characterized by the production of IL-4,
104 IL-5, and IL-13) compromises control of pulmonary fungal burden (26) and facilitates dis-
105 semination to the central nervous system (4, 26).
106
107 We hypothesized that the protracted host clearance of the *uxt1*Δ *uxt2*Δ mutant reflected
108 an altered host immune response to cells that display reduced xylose. To assess the host
109 response, we first analyzed cytokine levels over time in lung homogenates from mice

110 infected with WT or *uxt1*Δ *uxt2*Δ strains (Fig. 1). In mice infected with WT cryptococci, we
111 observed a strong Th2-type response, with significant induction of IL-4 and IL-5, over the
112 15 days prior to sacrifice (Fig. 1D, Fig. 1E). Other proinflammatory cytokines (IL-1α, IL-
113 1β, IL-6) were modestly increased (Supp. Fig. 1). In contrast, *uxt1*Δ *uxt2*Δ cells elicited a
114 more quiescent Th2 cytokine response at early stages of infection. Furthermore, at the
115 peak of fungal burden in *uxt1*Δ *uxt2*Δ-infected mice (day 63, Fig. 1A), there was a signif-
116 icant increase in the Th1 polarizing cytokine IL-12p40 compared to the levels observed
117 in naïve lungs (Fig. 1F); IL-12p40 levels then slowly declined, along with fungal burden.
118 Although the levels of IFNγ and TNFα in mutant-infected mice resembled those in the
119 lungs of naïve mice (Fig. 1G, Fig. 1H), IL-17 trended higher at the peak of infection (Fig.
120 1I). Overall, while WT infection rapidly induced non-protective Th2 responses, infection
121 with *uxt1*Δ *uxt2*Δ failed to do so (even at the peak of fungal burden) and instead promoted
122 the sustained induction of IL-12p40 and increased production of IL-17.
123
124 To measure the host adaptive immune response to *uxt1*Δ *uxt2*Δ, we used flow cytometry
125 to count lymphocytes in the lungs of mice infected with WT or *uxt1*Δ *uxt2*Δ cells. By 15
126 dpi, the B cell fraction of viable leukocytes in mutant-infected mice significantly exceeded
127 the value for WT-infected mice (Fig. 2A); this fraction further increased as mutant infection
128 progressed, to peak at over 30%. The same pattern was seen for $CD4^+$ and $CD8^+$ T cells
129 (Fig. 2B, Fig. 2C), initiating even earlier (at 12 dpi) and remaining high throughout the
130 time course. The total numbers of cells in all three populations remained elevated through
131 126 dpi (Fig. 2A-C, right), although they subsequently declined.
132

133 *Survival of uxt1Δ uxt2Δ-infected mice is dependent on T cells*

134 Because our results suggested that T and B cells play a protective role that contributes
135 to the prolonged survival of *uxt1*Δ *uxt2*Δ-infected mice, we next examined whether abla-
136 tion of these cell types altered the course of infection. Because the mouse strains used
137 for these studies were engineered in the C57BL/6 background, we included infections of
138 this strain as controls. C57BL/6 mice are less resistant to *C. neoformans* than the A/JCr
139 mice used above (27), as shown by their eventual susceptibility to *uxt1*Δ *uxt2*Δ infection
140 (Fig. 2D, solid black line). Notably, *Rag1*-/- mice in this background were significantly
141 more susceptible to the mutant fungi: all succumbed by 55 dpi (Fig 2D; solid blue line).
142 These animals still survived longer than WT-infected mice, possibly due to the slightly
143 slower growth of the mutant which we previously observed (21).

144

145 Since *Rag1*-/- mice lack both T and B cells, we also infected mice deficient in either T
146 cells (*TCRβ* -/-) or B cells (*μMT*) with *uxt1*Δ *uxt2*Δ cryptococci. B cell deficient mice ex-
147 hibited a more protracted course of disease than *Rag1*-/- animals, succumbing over an
148 85-day period (Fig. 2D, solid green line), while mice lacking only T cells succumbed to
149 infection with kinetics similar to those of the *Rag1*-/- mice (Fig. 2D, solid red line). In con-
150 trast, all mice inoculated with WT *C. neoformans* succumbed by 20 dpi (Fig. 2D; dashed
151 lines). Of this group, *Rag1*-/- and *TCRβ*-/- mice still succumbed slightly faster than
152 C57BL/6 and μMT mice (Fig. 2D). Together, these data show that T cells are the promi-
153 nent cell type responsible for increased survival of *uxt1*Δ *uxt2*Δ-infected mice, although
154 B cells may play a lesser role in protection.

155

156 *Reduced surface xylose of C. neoformans stimulates DC activation*

157 The antigen-driven activation of DCs is critical to induce protective immunity against *C.*
158 *neoformans* (28) and it is likely that their consequent cytokine and chemokine production
159 are responsible for T cell recruitment (23). We speculated that an enhanced DC response
160 to xylose-deficient fungi could explain the rise in T cells during *uxt1*Δ *uxt2*Δ infection (Fig.
161 2), even in the absence of expanded numbers of DCs (Fig. 3A). To test this idea, we grew
162 bone marrow derived DCs, stimulated them for 24 hours with heat-killed *C. neoformans*,
163 and measured the production of pro-inflammatory cytokines. In these studies we used
164 WT fungi, which display antigens modified with Xyl, or *uxt1*Δ *uxt2*Δ fungi, which are im-
165 paired in these modifications. We also tested strains with individual *uxt* mutations: *uxt1*Δ
166 shows an intermediate level of Xyl utilization while *uxt2*Δ resembles WT (21). Finally, we
167 assayed *uxs1*Δ cells, which lack all Xyl modification because they cannot synthesize
168 UDP-Xyl (29), and an acapsular control strain (*cap59*Δ) known to induce a potent DC
169 response (30).

170

171 We found that bone marrow derived DCs (BMDCs) cultured with *uxt1*Δ *uxt2*Δ cells re-
172 leased high levels of IL-1β and IL-6, comparable to the levels observed following expo-
173 sure to a completely acapsular control strain, *cap59*Δ (Fig. 3B-C). In contrast, individual
174 *uxt* mutants and *uxs1*Δ induced IL-1β and IL-6 levels similar to those induced by WT fungi
175 (close to background levels; Fig. 3B-C). TNF-α and IL-12p40 similarly showed the great-
176 est response upon challenge with *uxt1*Δ *uxt2*Δ, with levels like those induced by the acap-
177 sular strain, although a slight increase was also noted with other xylose-deficient strains
178 (*uxt1*Δ and *uxs1*Δ; Fig. 3D-E)). These results indicate that early interaction with DCs and

179 consequent induction of proinflammatory cytokines are influenced by the surface Xyl ex-
180 pression of *C. neoformans*.
181
182 *The cellular response to cryptococcal infection includes the development of inducible*
183 *bronchus-associated lymphoid tissue (iBALT)*
184 Our data suggested that *uxt1*Δ *uxt2*Δ mutant cells stimulate elevated production of pro-
185 inflammatory cytokines by DCs, which in turn significantly increases the T and B cells in
186 infected lungs (in both absolute numbers and as a fraction of total leukocytes). Flow cy-
187 tometry, however, provides no information as to the distribution of these cell populations
188 within the lung. To futher probe the cellular immune response, we therefore examined
189 lung histology, focusing on late time points of infection: 15 dpi for mice infected with WT
190 fungi and 126 and 189 dpi for *uxt1*Δ *uxt2*Δ-infected mice (also including 15 dpi to allow
191 direct comparison to WT). We used Movat's stain for these studies (Fig. 4), because the
192 Alcian Blue component stains cryptococcal cell walls and capsules turquoise, allowing
193 visualization of fungi as well as of host cells (31). In WT-infected mice at 15 dpi we saw
194 the typical pattern of overwhelming fungal burden throughout the lung, with little organized
195 inflammation (32). The tissue architecture was largely destroyed and there was a prepon-
196 derance of enlarged fungi with thick capsules. In contrast, mutant-infected mice at the
197 same time point showed relatively preserved tissue architecture, with limited regions of
198 organized inflammation. Most cryptococci were restricted to these areas and overall fun-
199 gal burden was noticeably lower, as expected for this mutant (Fig. 1A). By 126 dpi of
200 infection with mutant fungi, the regions of inflammation were larger and more highly con-
201 solidated; fungi were rarely observed in other areas of the lung. The last time point of

202 mutant infection (189 dpi) looked similar, although inflammation appeared slightly re-
203 duced, consistent with the decrease in B and T cells that we observed at that time point
204 (Fig. 2). Lymphoid structures were also less dense; fungi were less restricted to the cen-
205 ters of these regions and occasionally appeared in lung tissue beyond them.
206
207 In both groups of mice (WT- and mutant-infected), we noted distinctive lymphocytic accu-
208 mulations proximal to the basal side of the bronchial epithelium (Fig. 4). To probe these
209 structures, we stained lung sections for T cells (CD3), B cells (B220), and plasma cells
210 (IgG). In all samples we observed B cell follicles surrounded by $CD3^+$ T cell cuffs (Fig 5A),
211 suggestive of inducible bronchus-associated lymphoid tissue (iBALT) (24). Consistent
212 with identification as iBALT, these structures stained positive for CXCL13 (Fig. 5B).
213
214 To examine iBALT development, we performed blinded morphometric analysis of lung
215 tissue from mice infected with WT and mutant cryptococci. At 15 dpi with WT fungi, we
216 observed numerous iBALT structures, with compact B cell follicles surrounded by T cells
217 (Figs. 5C-E). In contrast, B cell follicles were considerably fewer and less organized at
218 the same time point in mice infected with the *uxt1*Δ *uxt2*Δ strain (Figs. 5C-E). The limited
219 formation of iBALT structures was also characterized by increased peri-vascular accumu-
220 lation of T cells (Fig. 5A) and decreased production of CXCL13 (Fig. 5B, Fig. 5F). By 126
221 dpi with *uxt1*Δ *uxt2*Δ, however, although iBALT structures were still less abundant than
222 those found in WT infection (Fig. 5C), their average B cell follicle size was significantly
223 larger (Fig. 5D). Additionally, the *uxt1*Δ *uxt2*Δ iBALT was more organized, with reduced
224 T cell cuffing (Fig. 5E), increased CXCL13 (Fig. 5F) and more IgG^+ plasma cells (Fig. 5A).

225 By 189 dpi, these structures regressed slightly, consistent with the reduced lymphocyte
226 infiltration, cytokine levels, and fungal burden at this time point. WT cryptococci thus in-
227 duce robust early formation of iBALT, while the *uxt1*Δ *uxt2*Δ mutant induces delayed but
228 ultimately larger and better organized iBALT.
229
230
231 **DISCUSSION**
232
233 We wished to investigate the unexpected observation that a mutant strain of *C. neofor-*
234 *mans*, despite significant defects in surface glycoconjugates, nevertheless persisted for
235 many months in infected mice. We found that *uxt1*Δ *uxt2*Δ cells showed an initial delay
236 after intranasal infection, but then began to accumulate slowly, eventually rising to a
237 modest peak, at which time (63 dpi) we also observed limited dissemination. The lung
238 burden then began to gradually decline, although by the end point of the study (189 dpi)
239 only three of ten animals had cleared the infection.
240
241 The *uxt1*Δ *uxt2*Δ mutant induced a generally subdued pulmonary immune response
242 compared to that induced by WT cryptococci. Notably, levels of IL-12p40, a cytokine
243 normally required for inducing a protective response against *C. neoformans* (33), were
244 elevated at 63 dpi and beyond (Fig. 1F); this may facilitate subsequent resolution of the
245 *uxt1*Δ *uxt2*Δ infection. The rise in IL-12p40 could reflect an increase in either IL-23 or IL-
246 12 (34), which stimulate Th17 and Th1 type responses, respectively. Since we observed

247 a trend towards increased IL-17 at 63 dpi, but no difference in IFN-γ levels, IL-12p40
248 was more likely associated with a Th17 response.
249
250 In terms of overall lung histology, the early host response of mutant-infected mice was
251 limited. By 128 dpi it had become more organized, with all fungi apparently contained
252 within inflammatory structures, although there was a slight degradation of fungal control
253 by the last time point imaged (189 dpi). We specifically quantitated the temporal pro-
254 gression for iBALT and found that B-cell follicles at the earliest time point of mutant in-
255 fections (15 dpi) were sparse and small compared to 15 dpi wild-type iBALT, with larger
256 T cell cuffs and smaller areas of CXCL13 staining. By 126 dpi, however, their follicle
257 size and CXCL3 staining had surpassed WT levels, although these parameters re-
258 gressed somewhat by 189 dpi. The development of iBALT, therefore, paralleled the abil-
259 ity of the host immune response to physically contain cryptococci within inflammatory
260 structures in the lung.
261
262 DCs reacted more strongly to *uxt1*Δ *uxt2*Δ than to WT *in vitro*, releasing greater amounts
263 of pro-inflammatory cytokines (Fig. 3B-E), even though the global cytokine response to
264 the mutant was less perturbed (Fig 1D-I). These cytokines may directly or indirectly lead
265 to the increased recruitment of T and B cells in *uxt1*Δ *uxt2*Δ infection (Fig. 2A-C) and
266 perhaps accelerate compartmentalization into compact B cell follicles and discrete T cell
267 areas in iBALT (Fig 5). Such differences in cellular composition and organization, coupled
268 with differences in the local cytokine production, may confer distinct properties on the

269 iBALT induced by WT and *uxt1*Δ *uxt2*Δ, influencing their ability to protect against *C.*
270 *neoformans*.
271
272 We expected that the highly immunostimulatory behavior of *uxt1*Δ *uxt2*Δ *in vitro* reflected
273 the lack of Xyl modifications on its surface glycoconjugates, a consequence of the ab-
274 sence of UDP-Xyl transport into the secretory compartment. We were surprised, there-
275 fore, that mutants unable to synthesize UDP-Xyl (*uxs1*Δ), which similarly lack Xyl modifi-
276 cations on secreted glycoconjugates, did not phenocopy this broad and robust DC re-
277 sponse. This suggests that Uxs1 itself is required for the strong response seen in the
278 absence of xylosylation in the secretory pathway. It may be that this protein plays addi-
279 tional roles unrelated to glycosylation (35), or that the stimulatory component is depend-
280 ent on cytosolic UDP-Xyl, rather than UDP-Xyl that has been transported into the secre-
281 tory pathway.
282
283 Unlike encapsulated strains, *C. neoformans* mutants lacking capsule induce the upregu-
284 lation of multiple genes involved in cytokine responses and enhance antigen processing
285 and presentation by DCs (36). Interestingly, the cytokine levels induced in DC by the
286 *uxt1*Δ *uxt2*Δ mutant were similar to those induced by the acapsular mutant *cap59*Δ (Fig
287 4A-C). Xyl may thus be critical for the immune suppressive effects normally exerted by
288 capsule material. The mechanisms behind the robust DC activation seen in these two
289 mutants, including the cellular receptors and fungal components responsible, remain to
290 be determined. It is possible that the *uxt1*Δ *uxt2*Δ mutant lacks immune suppressive

291 mechanisms that are present in WT *C. neoformans* infection, and therefore induces ro-
292 bust cytokine responses and consequent recruitment of T and B cells that stimulate iBALT
293 formation and limit early infection.
294
295 In this study, we report for the first time that *C. neoformans* infection triggers iBALT for-
296 mation. To our knowledge, the only other fungus reported to induce iBALT is *Pneumo-*
297 *cystis* (37). Notably, the iBALT detected in our experimental infections resembles sub-
298 pleural nodules that have been observed in cryptococcosis patients (38), although fur-
299 ther examination will be necessary to establish the similarities between histological fea-
300 tures of inflammatory cell infiltration in mice and humans. Although iBALT formation oc-
301 curred in mice infected with both mutant and WT fungi, it was inadequate to defend
302 against the overwhelming fungal burden that rapidly develops in a standard murine
303 model of cryptococcal infection. It may be that lower inocula would shift the balance in
304 favor of the host. In any event, the kinetics of iBALT formation and its organization are
305 dependent on virulence factors of the pathogen. Future studies will be needed to fully
306 delineate the molecular host-pathogen interactions that drive iBALT formation following
307 *C. neoformans* infection and the magnitude of the role that iBALT plays; in this regard
308 specific chemokine deficient mice, such as CXCL-13 deficient animals that lack the abil-
309 ity to induce iBALT structures (39), may be useful.
310

311 **MATERIALS AND METHODS**

312 *Fungal strains*

313 *C. neoformans* strains (Table S1) were grown at 30 °C in YPD medium (1% [wt/vol] yeast
314 extract, 2% [wt/vol] peptone, 2% [wt/vol] dextrose) with shaking (230 rpm) or on YPD agar
315 plates (YPD medium with 2% [wt/vol] agar) supplemented with the following antibiotics as
316 appropriate: 100 µg/ml nourseothricin (NAT; Werner BioAgents) or Geneticin (G418; Invi-
317 trogen).

318

319 *Mice*

320 C57BL/6J (RRID: IMSR_JAX:000664) and A/JCr (RRID: IMSR_CRL:563) mice were ob-
321 tained from Jackson Laboratory. *Rag1*-/- (RRID: IMSR_JAX:002216), *TCRβ*-/- (RRID:
322 IMSR_JAX:002118), and µMT mice (RRID: IMSR_JAX:002288) (all on C57BL/6 back-
323 ground) were generously provided by Dr. Michael Diamond and Dr. Wayne Yokoyama
324 (Washington University School of Medicine); breeders were originally purchased from
325 Jackson Laboratory. All mice were 6 to 8 weeks old at the time of infection. A/JCr mice
326 were female; male and female mice were used for the other strains with gender and age
327 matched C57BL/6 controls.

328

329 *Ethics statement*

330 All animal protocols were reviewed and approved by the Animal Studies Committee of
331 the Washington University School of Medicine and conducted according to National Insti-
332 tutes of Health guidelines for housing and care of laboratory animals.

333

334 *C. neoformans infection*

335 Fungal strains were cultured overnight (O/N) and diluted to 10^6 cells/mL in sterile PBS.
336 Mice were intranasally inoculated with a 50 μL aliquot, and then weighed and monitored
337 daily. Infected mice were sacrificed if they lost >20% relative to peak weight or at specified
338 time points. At the time of sacrifice, mice were perfused intracardially with 10 mL sterile
339 PBS, and organs were processed as described below for fungal burden, histology, flow
340 cytometric analysis, and cytokine measurements.

341

342 *Organ burden and cytokines*

343 Brain and spleen homogenates were harvested and plated for CFU at the specified time
344 points. 50 μL aliquots of the left lung homogenates (V_T = 1 mL) were similarly plated for
345 CFUs. The remaining sample was assayed for pulmonary cytokine levels using the Bio-
346 Plex Protein Array System (Bio-Rad Laboratories). Briefly, the lung homogenates were
347 mixed with an equal volume of PBS/0.1% Triton 100x/2x protease inhibitor (Pierce EDTA-
348 free protease inhibitor; Thermo Scientific), vortexed for 3 seconds, and clarified by cen-
349 trifugation (2500 x g, 10 min). Supernatant fractions were then assayed using the Bio-
350 Plex Pro Mouse Cytokine 23-Plex (Bio-Rad Laboratories) for the presence of IL-1α, IL-
351 1β, IL-2, IL-3, IL-4, IL-5, IL-6, IL-9, IL-10, IL-12 (p40), IL-12 (p70), IL-13, IL-17A, granulo-
352 cyte colony stimulating factor (G-CSF), granulocyte monocyte colony stimulating factor
353 (GM-CSF), interferon-γ (IFN-γ), CXCL1/keratinocyte-derived chemokine (KC),
354 CCL2/monocyte chemotactic protein-1 (MCP-1), CCL3/macrophage inflammatory pro-
355 tein-1α (MIP-1α), CCL4/MIP-1β, CCL5/regulated upon activation normal T cell expressed
356 and secreted (RANTES), and tumor necrosis factor-α (TNF-α).

357

358 *Tissue staining and histologic analysis*

359 Mice were perfused intracardially with sterile PBS, and the lungs inflated with 10% forma-
360 lin. Lung tissue was then fixed O/N in 10% formalin and submitted to the Washington
361 University Developmental Biology Histology Core for paraffin-embedding and sectioning.
362 Immunofluorescence staining for B cells (APC-conjugated rat anti-mouse CD45R/B220,
363 clone RA3-6B2, BD Biosciences, RRID: AB_627078), T cells (CD3-ε, clone M-20, Santa
364 Cruz Biotechnology, RRID: AB_631129), Ig G^+ plasma cells (FITC-donkey anti-mouse Ig
365 G, Jackson ImmunoResearch Laboratories, RRID: AB_2340796), and CXCL13-produc-
366 ing cells (goat α-mouse CXCL13, AF470, R&D Systems, RRID: AB_355378) was per-
367 formed as in Ref (37). Images were taken with a Zeiss Axioplan2 microscope and rec-
368 orded with a Hamamatsu camera. Blinded morphometric analysis of lung structures was
369 performed with the outline tool of Zeiss Axiovision software. Additional sections were
370 stained with Movat's pentachrome stain by the Washington University Pulmonary Mor-
371 phology Core.

372

373 *Flow cytometric analysis*

374 The right lung of individual mice was enzymatically digested (in 5 mL RPMI with 1 mg/mL
375 collagenase type IV) at 37 °C with shaking (230 rpm) for 30 min, and then sequentially
376 passed through sterile 70 and 40 µm pore nylon strainers (BD Biosciences, San Jose,
377 CA). Red blood cells in the samples were lysed by treatment for 3 min on ice with 5 mL
378 ammonium-chloride-potassium lysing buffer (8.024 g/L NH_4Cl, 1.001 g/L $KHCO_3$, 2.722
379 mg/L EDTA•Na_2 $2H_2O$), followed by the addition of 2 volumes of PBS. The remaining cells

380 were pelleted (1000 x g, 5 min, 4 °C), washed twice with PBS, diluted to 10^6 cells/mL in
381 PBS, and stained with LIVE/DEAD fixable blue dead cell stain (1:1000; Thermo Scien-
382 tific). Following incubation in the dark for 30 min at 4 °C, cells were washed with PBS and
383 FACS buffer (2% fetal bovine serum in PBS) before resuspension in FACS buffer. Sam-
384 ples were then blocked with CD16/CD32 (1:500; Fc Block™; BD Biosciences, RRID:
385 AB_394656) for 5 min and incubated for 30 min with optimal concentrations of fluoro-
386 chrome-conjugated antibodies (Table S2) diluted in Brilliant Stain Buffer (BD Biosci-
387 ences). After three washes with FACS buffer, the cells were fixed in 2% formalde-
388 hyde/FACS buffer. For data acquisition, >50,000 events were collected on a BD LSRFor-
389 tessa X-20 flow cytometer (BD Biosciences), and the data were analyzed with FlowJo
390 V10 (Fig. S1; TreeStar). The absolute number of cells in each leukocyte subset was de-
391 termined by multiplying the absolute number of $CD45^+$ cells by the percentage of cells
392 stained by fluorochrome-labeled antibodies for each cell population analyzed.
393
394 *Isolation of bone marrow derived cells*
395 Bone marrow was flushed from the femurs and tibiae of C57BL/6 mice using RPMI. Cells
396 were collected (1000 x g, 5 min, 4°C), resuspended in RPMI, and counted using a hemo-
397 cytometer. To prepare bone marrow derived dendritic cells (BMDCs), 2 x 10^6 bone mar-
398 row cells were plated in 10 mL R10 medium (10% FBS, 0.4% Penicillin-Streptomycin, 2
399 mM L-glutamate, 50 μM 2-β-mercaptoethanol in RPMI) supplemented with 1 ng/mL GM-
400 CSF, and incubated at 37 °C and 5% CO_2. Medium was changed 3 and 6 days after
401 plating, and cells were harvested on day 8. BMDCs were enriched by depletion of BMMs

402 using biotinylated α-F4/80 antibody (eBioscience, RRID: AB_466657) and anti-biotin con-
403 jugated magnetic beads (Miltenyi Biotec). The BMDCs in the flow through were positively
404 selected using α-CD11c magnetic beads according to the manufacturer's protocol (Mil-
405 tenyi Biotec).
406
407 *Dendritic cell assays*
408 To assay the ability of fungal strains to activate BMDCs, *C. neoformans* strains of interest
409 were grown O/N, washed in PBS, and incubated at 65 °C for 15 min to heat kill (HK) the
410 fungi. BMDCs and HK fungi (10^6 cells of each) were then co-incubated for 24 h, sedi-
411 mented, and the supernatant fractions transferred to 1.5 mL centrifuge tubes containing
412 10 µL of 100x protease inhibitor (ThermoScientific). IL-1β, IL-6, and TNF-α levels in su-
413 pernatants were determined by ELISA according to the manufacturer's protocol (R&D
414 systems).
415
416 *Statistical analysis*
417 Each experiment was performed a minimum of two times. Statistical analyses were con-
418 ducted using GraphPad Prism version 6.0f (GraphPad Software). All studies comparing
419 two groups were analyzed with a Student's t-test. Those with three or more groups were
420 compared using an ordinary one-way ANOVA with Tukey's *post-hoc* test. $p < 0.05$ was
421 considered statistically significant.
422
423 **ACKNOWLEDGEMENTS**

We thank members of the Doering laboratory for helpful discussions and assistance with experiments. We also thank Dr. Thomas R. Kozel (University of Nevada School of Medicine) for anti-GXM monoclonal antibody, and Dr. Michael Diamond and Dr. Wayne Yokoyama for immune deficient mouse lines.

This work was funded by National Institutes of Health grants R21 AI109623 and R01 AI102882 to TLD. LXL was partly supported by a National Research Science Award (T32 GM007200), a Sondra Schlesinger Graduate Fellowship (Washington University St. Louis Microbiology Department), and a National Institute of Allergy and Infectious Diseases fellowship (F30 AI120339). CRH was partly funded by a National Institute of Allergy and Infectious Diseases training grant (T32 AI007172). SAK and JRM were supported by NIH grant R01 AI111914. The funders had no role in study design, data collection and interpretation, or the decision to submit the work for publication.

AUTHOR CONTRIBUTIONS

Conceptualization, LXL, CRH, SAK, and TLD; Methodology, LXL, CRH, JRM, SAK, TLD; Investigation, LXL, CRH, and JRM; Writing – Original Draft, LXL and CRH; Writing – Review & Editing, CRH, JRM, SAK, and TLD; Funding Acquisition, LXL, SAK and TLD; Resources, SAK and TLD; Supervision, SAK and TLD.

DECLARATION OF INTERESTS

LXL, CRH, JRM, SAK and TLD have no interests to declare

447 **References**

448

449 1. Kwon-Chung KJ, Fraser JA, Doering TL, Wang Z, Janbon G, Idnurm A, Bahn YS.
450 2014. *Cryptococcus neoformans* and *Cryptococcus gattii,* the etiologic agents of
451 cryptococcosis. Cold Spring Harb Perspect Med 4:a019760.

452 2. Denning DW. 2016. Minimizing fungal disease deaths will allow the UNAIDS target
453 of reducing annual AIDS deaths below 500 000 by 2020 to be realized. Philos
454 Trans R Soc Lond B Biol Sci 371.

455 3. Rajasingham R, Smith RM, Park BJ, Jarvis JN, Govender NP, Chiller TM, Denning
456 DW, Loyse A, Boulware DR. 2017. Global burden of disease of HIV-associated
457 cryptococcal meningitis: an updated analysis. Lancet Infect Dis
458 doi:10.1016/S1473-3099(17)30243-8.

459 4. Wozniak KL, Levitz SM. 2011. T cell and dendritic cell immune responses to
460 Cryptococcus, p p 387-396. *In* Heitman J, Kozel TR, Kwon-Chung KJ, Perfect JR,
461 Casadeval A (ed), Cryptococcus. ASM Press, Washington, DC.

462 5. Zhang Y, Wang F, Tompkins KC, McNamara A, Jain AV, Moore BB, Toews GB,
463 Huffnagle GB, Olszewski MA. 2009. Robust Th1 and Th17 immunity supports
464 pulmonary clearance but cannot prevent systemic dissemination of highly virulent
465 *Cryptococcus neoformans* H99. Am J Pathol 175:2489-500.

466 6. Wozniak KL, Hardison SE, Kolls JK, Wormley FL. 2011. Role of IL-17A on
467 resolution of pulmonary *C. neoformans* infection. PLoS One 6:e17204.

468 7. Murdock BJ, Huffnagle GB, Olszewski MA, Osterholzer JJ. 2014. Interleukin-17A
469 enhances host defense against cryptococcal lung infection through effects

470 mediated by leukocyte recruitment, activation, and gamma interferon production.
471 Infect Immun 82:937-48.
472 8. Schulze B, Piehler D, Eschke M, von Buttlar H, Kohler G, Sparwasser T, Alber G.
473 2014. CD4(+) FoxP3(+) regulatory T cells suppress fatal T helper 2 cell immunity
474 during pulmonary fungal infection. Eur J Immunol 44:3596-604.
475 9. Wiesner DL, Smith KD, Kotov DI, Nielsen JN, Bohjanen PR, Nielsen K. 2016.
476 Regulatory T cell induction and retention in the lungs drives suppression of
477 detrimental type 2 Th cells during pulmonary cryptococcal infection. J Immunol
478 196:365-74.
479 10. Wiesner DL, Specht CA, Lee CK, Smith KD, Mukaremera L, Lee ST, Lee CG, Elias
480 JA, Nielsen JN, Boulware DR, Bohjanen PR, Jenkins MK, Levitz SM, Nielsen K.
481 2015. Chitin recognition via chitotriosidase promotes pathologic type-2 helper T
482 cell responses to cryptococcal infection. PLoS Pathog 11:e1004701.
483 11. Wolfert MA, Boons GJ. 2013. Adaptive immune activation: glycosylation does
484 matter. Nat Chem Biol 9:776-84.
485 12. Zaragoza O, Rodrigues ML, De Jesus M, Frases S, Dadachova E, Casadevall A.
486 2009. The capsule of the fungal pathogen *Cryptococcus neoformans*. Adv Appl
487 Microbiol 68:133-216.
488 13. Yauch LE, Lam JS, Levitz SM. 2006. Direct inhibition of T-cell responses by the
489 Cryptococcus capsular polysaccharide glucuronoxylomannan. PLoS Pathog
490 2:e120.
491 14. Agustinho DP, Miller LC, Li LX, Doering TL. 2018. Peeling the onion: the outer
492 layers of *Cryptococcus neoformans*. Mem Inst Oswaldo Cruz 113:e180040.

493 15. Wang ZA, Li LX, Doering TL. 2018. Unraveling synthesis of the cryptococcal cell
494 wall and capsule. Glycobiology 28:719-730.
495 16. Cherniak R, Valafar H, Morris LC, Valafar F. 1998. *Cryptococcus neoformans*
496 chemotyping by quantitative analysis of 1H nuclear magnetic resonance spectra
497 of glucuronoxylomannans with a computer-simulated artificial neural network. Clin
498 Diagn Lab Immunol 5:146-59.
499 17. Castle SA, Owuor EA, Thompson SH, Garnsey MR, Klutts JS, Doering TL, Levery
500 SB. 2008. Beta1,2-xylosyltransferase Cxt1p is solely responsible for xylose
501 incorporation into *Cryptococcus neoformans* glycosphingolipids. Eukaryot Cell
502 7:1611-5.
503 18. Klutts JS, Levery SB, Doering TL. 2007. A beta-1,2-xylosyltransferase from
504 *Cryptococcus neoformans* defines a new family of glycosyltransferases. J Biol
505 Chem 282:17890-9.
506 19. Park JN, Lee DJ, Kwon O, Oh DB, Bahn YS, Kang HA. 2012. Unraveling unique
507 structure and biosynthesis pathway of N-linked glycans in human fungal pathogen
508 *Cryptococcus neoformans* by glycomics analysis. J Biol Chem 287:19501-15.
509 20. Lee DJ, Bahn YS, Kim HJ, Chung SY, Kang HA. 2015. Unraveling the novel
510 structure and biosynthetic pathway of O-linked glycans in the Golgi apparatus of
511 the human pathogenic yeast *Cryptococcus neoformans*. J Biol Chem 290:1861-
512 73.
513 21. Li LX, Rautengarten C, Heazlewood JL, Doering TL. 2018. Xylose donor transport
514 is critical for fungal virulence. PLoS Pathog 14:e1006765.

515 22. Randall TD, Carragher DM, Rangel-Moreno J. 2008. Development of secondary
516 lymphoid organs. Annu Rev Immunol 26:627-50.
517 23. Hwang JY, Randall TD, Silva-Sanchez A. 2016. Inducible bronchus-associated
518 lymphoid tissue: taming inflammation in the lung. Front Immunol 7:258.
519 24. Moyron-Quiroz JE, Rangel-Moreno J, Kusser K, Hartson L, Sprague F, Goodrich
520 S, Woodland DL, Lund FE, Randall TD. 2004. Role of inducible bronchus
521 associated lymphoid tissue (iBALT) in respiratory immunity. Nat Med 10:927-34.
522 25. Geurts van Kessel CH, Willart MA, Bergen IM, van Rijt LS, Muskens F, Elewaut D,
523 Osterhaus AD, Hendriks R, Rimmelzwaan GF, Lambrecht BN. 2009. Dendritic
524 cells are crucial for maintenance of tertiary lymphoid structures in the lung of
525 influenza virus-infected mice. J Exp Med 206:2339-49.
526 26. Koguchi Y, Kawakami K. 2002. Cryptococcal infection and Th1-Th2 cytokine
527 balance. Int Rev Immunol 21:423-38.
528 27. Huffnagle GB, Boyd MB, Street NE, Lipscomb MF. 1998. IL-5 is required for
529 eosinophil recruitment, crystal deposition, and mononuclear cell recruitment during
530 a pulmonary *Cryptococcus neoformans* infection in genetically susceptible mice
531 (C57BL/6). J Immunol 160:2393-400.
532 28. Leopold Wager CM, Hole CR, Wozniak KL, Wormley FL, Jr. 2016. Cryptococcus
533 and Phagocytes: Complex Interactions that Influence Disease Outcome. Front
534 Microbiol 7:105.
535 29. Bar-Peled M, Griffith CL, Doering TL. 2001. Functional cloning and
536 characterization of a UDP-glucuronic acid decarboxylase: the pathogenic fungus

537 *Cryptococcus neoformans* elucidates UDP-xylose synthesis. Proc Natl Acad Sci U
538 S A 98:12003-12008.
539 30. Grijpstra J, Tefsen B, van Die I, de Cock H. 2009. The *Cryptococcus neoformans*
540 *cap10* and *cap59* mutant strains, affected in glucuronoxylomannan synthesis,
541 differentially activate human dendritic cells. FEMS Immunol Med Microbiol 57:142-
542 50.
543 31. Rittershaus PC, Kechichian TB, Allegood JC, Merrill AH, Jr., Hennig M, Luberto C,
544 Del Poeta M. 2006. Glucosylceramide synthase is an essential regulator of
545 pathogenicity of *Cryptococcus neoformans*. J Clin Invest 116:1651-9.
546 32. Gish SR, Maier EJ, Haynes BC, Santiago-Tirado FH, Srikanta DL, Ma CZ, Li LX,
547 Williams M, Crouch EC, Khader SA, Brent MR, Doering TL. 2016. Computational
548 Analysis Reveals a Key Regulator of Cryptococcal Virulence and Determinant of
549 Host Response. MBio 7.
550 33. Decken K, Kohler G, Palmer-Lehmann K, Wunderlin A, Mattner F, Magram J,
551 Gately MK, Alber G. 1998. Interleukin-12 is essential for a protective Th1 response
552 in mice infected with *Cryptococcus neoformans*. Infect Immun 66:4994-5000.
553 34. Oppmann B, Lesley R, Blom B, Timans JC, Xu Y, Hunte B, Vega F, Yu N, Wang
554 J, Singh K, Zonin F, Vaisberg E, Churakova T, Liu M, Gorman D, Wagner J,
555 Zurawski S, Liu Y, Abrams JS, Moore KW, Rennick D, de Waal-Malefyt R, Hannum
556 C, Bazan JF, Kastelein RA. 2000. Novel p19 protein engages IL-12p40 to form a
557 cytokine, IL-23, with biological activities similar as well as distinct from IL-12.
558 Immunity 13:715-25.

559 35. Billmyre RB, Applen Clancey S, Li LX, Doering TL, Heitman J. 2020. 5-
560 fluorocytosine resistance is associated with hypermutation and alterations in
561 capsule biosynthesis in Cryptococcus. Nat Commun 11:127.
562 36. Lupo P, Chang YC, Kelsall BL, Farber JM, Pietrella D, Vecchiarelli A, Leon F,
563 Kwon-Chung KJ. 2008. The presence of capsule in *Cryptococcus neoformans*
564 influences the gene expression profile in dendritic cells during interaction with the
565 fungus. Infect Immun 76:1581-9.
566 37. Eddens T, Elsegeiny W, Garcia-Hernadez ML, Castillo P, Trevejo-Nunez G,
567 Serody K, Campfield BT, Khader SA, Chen K, Rangel-Moreno J, Kolls JK. 2017.
568 Pneumocystis-driven inducible bronchus-associated lymphoid tissue formation
569 requires Th2 and Th17 immunity. Cell Rep 18:3078-3090.
570 38. Haugen RK, Baker RD. 1954. The pulmonary lesions in cryptococcosis with
571 special reference to subpleural nodules. Am J Clin Pathol 24:1381-90.
572 39. Slight SR, Rangel-Moreno J, Gopal R, Lin Y, Fallert Junecko BA, Mehra S, Selman
573 M, Becerril-Villanueva E, Baquera-Heredia J, Pavon L, Kaushal D, Reinhart TA,
574 Randall TD, Khader SA. 2013. CXCR5(+) T helper cells mediate protective
575 immunity against tuberculosis. J Clin Invest 123:712-26.
576

577 **FIGURES WITH LEGENDS**

578 **SUPPLEMENTARY FIGURES WITH LEGENDS**

579 **SUPPLEMENTARY TABLES AND REFERENCES**

580

FIGURES WITH LEGENDS

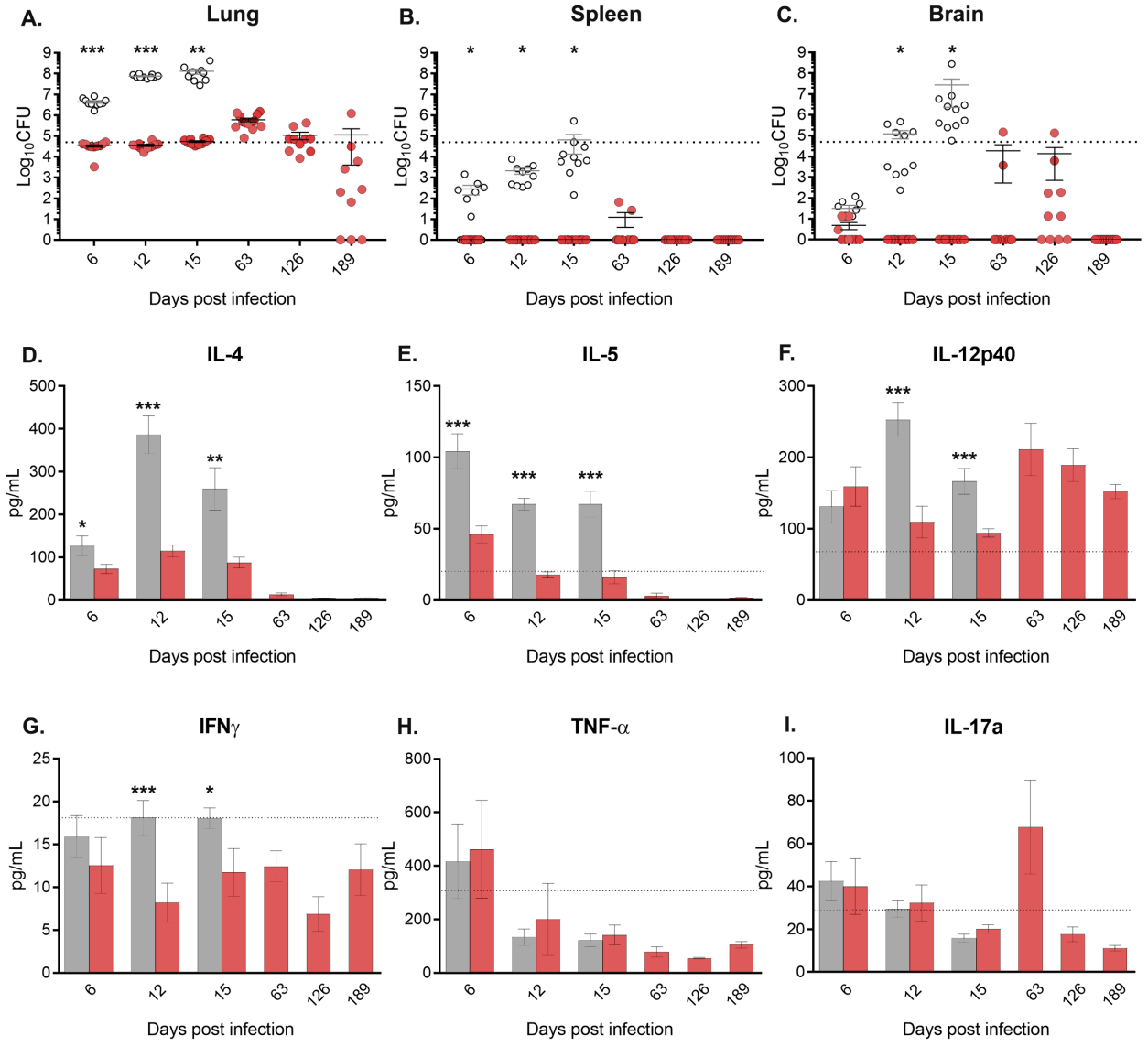

Figure 1. Fungal burden and pulmonary cytokine production in WT and *uxt1*Δ *uxt2*Δ mice. All panels show the combined results of two independent experiments (5 mice per group per experiment). (A-C) Tissue homogenates of infected A/JCr mice were plated for CFUs at the indicated dpi (open symbols, WT; red symbols, *uxt1*Δ *uxt2*Δ; dashed line, initial inoculum). Values from individual mice are plotted along with the mean ± SEM. (D-I) Cytokine levels in lung homogenates at the indicated dpi (dashed line, naïve; gray bars, WT; red bars, *uxt1*Δ *uxt2*Δ). *, $p < 0.05$; **, $p < 0.01$; ***, $p < 0.005$ for Student's t-test comparing WT to mutant.

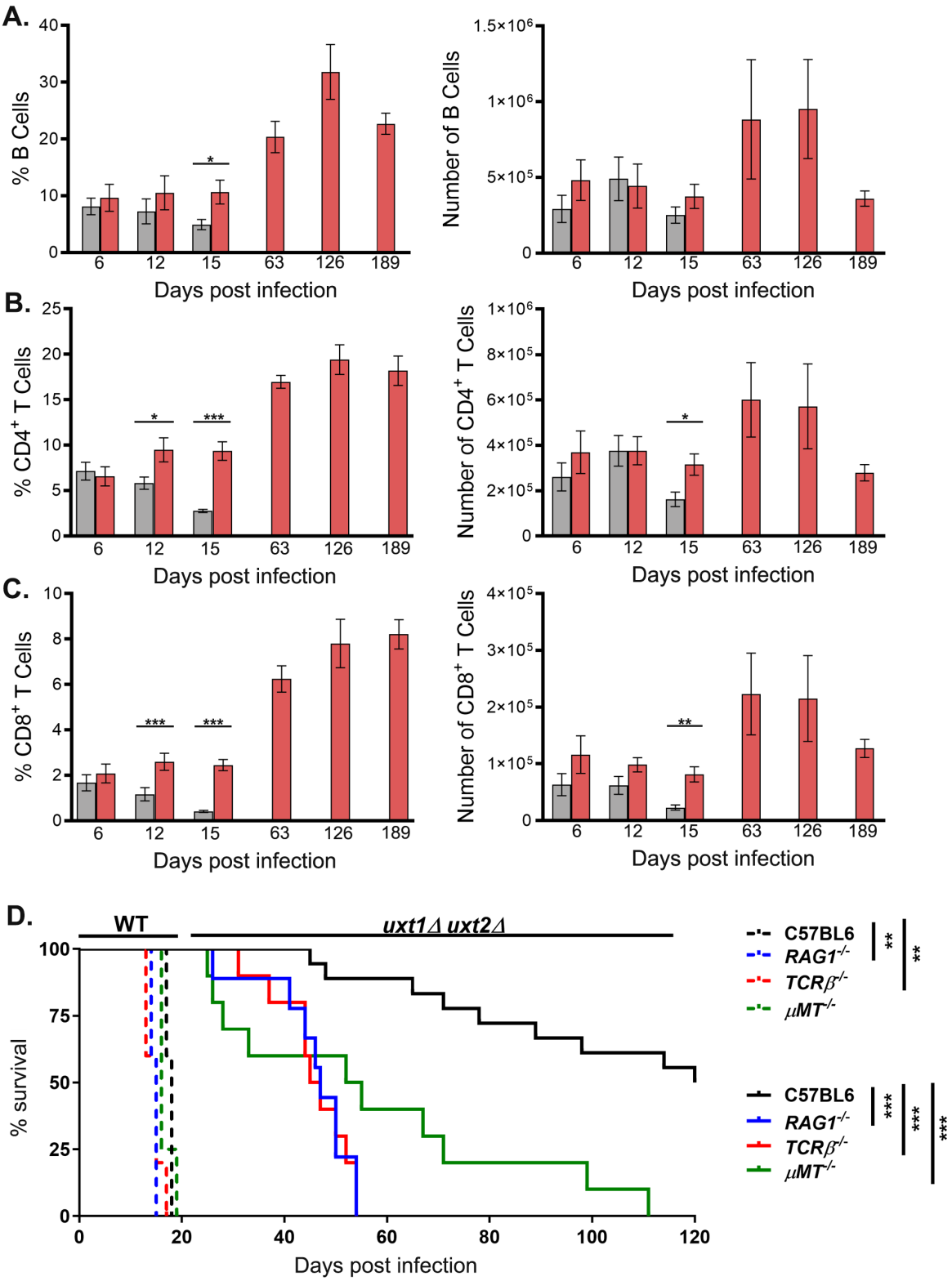

Figure 2. Accumulation of T and B cells in the lungs of mice infected with *uxt1*Δ *uxt2*Δ cells is required to prevent disease progression. CD19⁺ B cells (A), CD4⁺ T cells (B), and CD8⁺ T cells (C) were enumerated in the lungs of infected mice by flow cytometry (gray, WT; red, *uxt1*Δ *uxt2*Δ). Plotted are the combined mean ± SEM values from two independent experiments (5

mice per group per experiment). *, $p < 0.05$; **, $p < 0.01$; ***, $p < 0.005$ by Student's t-test. (D) Survival of mice after intranasal inoculation with 5×10^4 cells of WT (n = 5) or *uxt1*Δ *uxt2*Δ (n = 10). Results shown are combined from two independent experiments. **, $p < 0.01$; ***, $p < 0.005$ by the log-rank test.

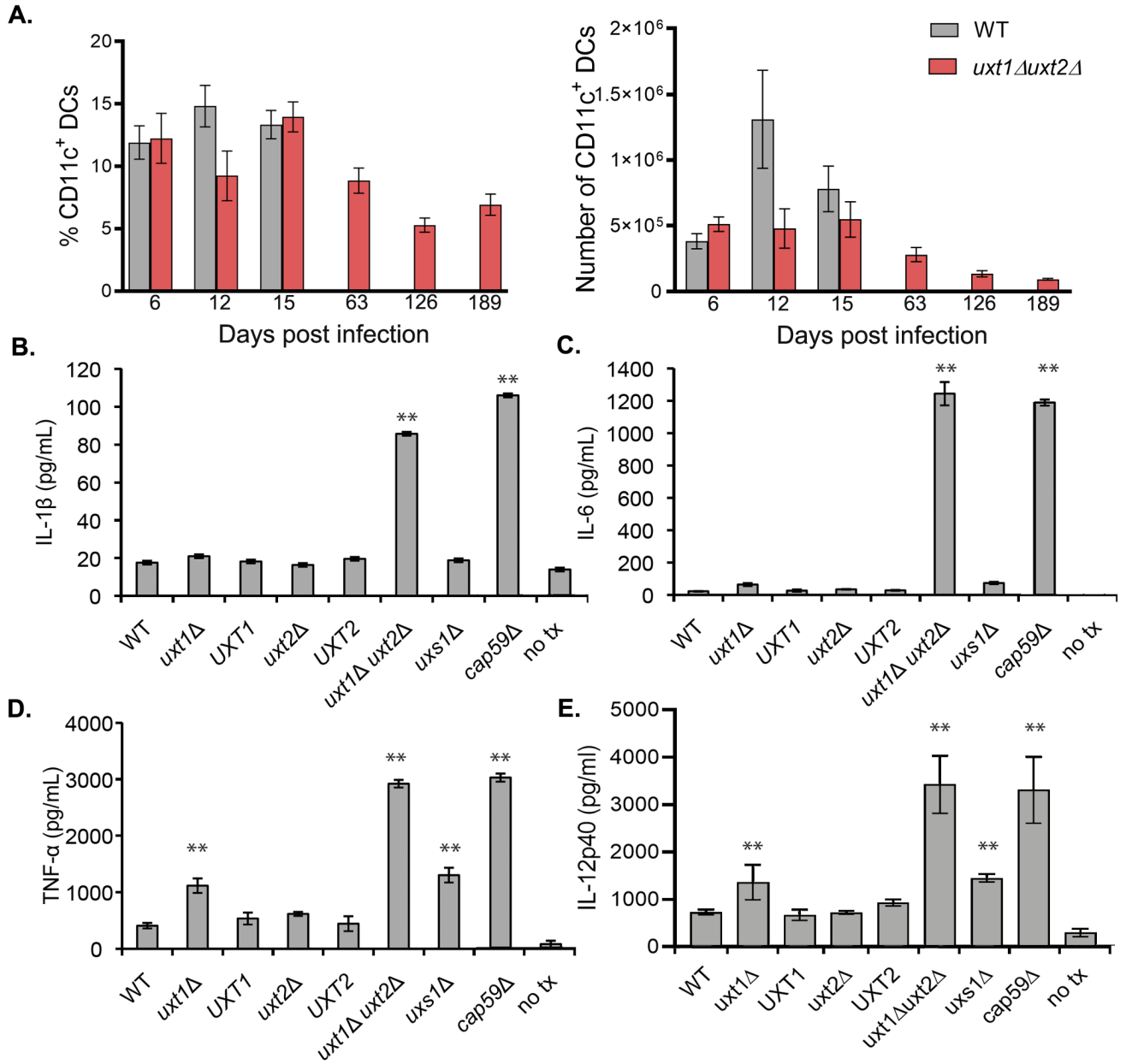

Figure 3. Cytokine production by dendritic cells stimulated with cryptococcal antigens. (A) CD11c+ DC populations in the lungs of infected mice were quantified by flow analysis. (B-E) DCs were co-incubated for 24 h with heat-killed cells of the strains indicated or subjected to no treatment (no tx) and levels of IL-1β (B), IL-6 (C), TNF-α (D), and IL-12p40 (E) in the supernatant were quantified by ELISA. Shown are the mean ± SD (n = 3) values for one representative experiment from five independent experiments that yielded similar results. **, $p < 0.01$ by one-way ANOVA with Tukey's post hoc test.

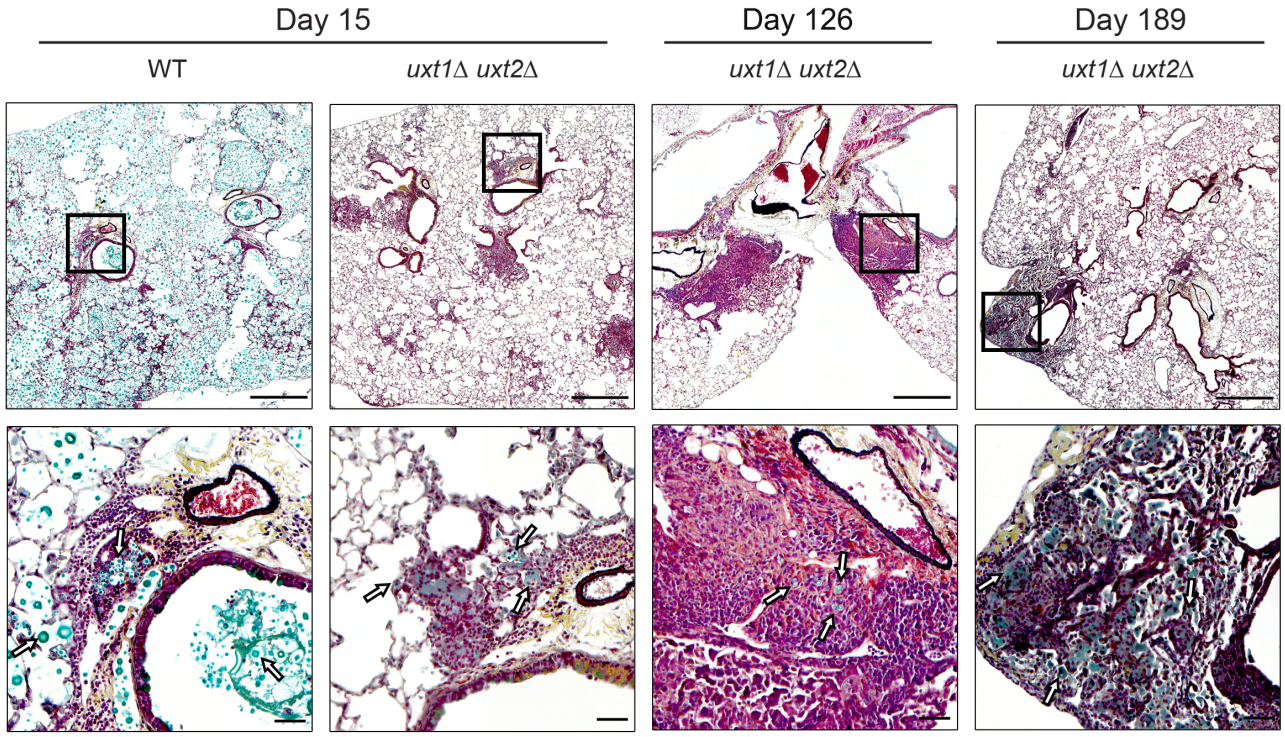

Figure 4. Mutant cryptococci are primarily restricted to lymphoid structures. Micrographs show Movat-stained lung sections from A/JCr mice infected with WT or *uxt1Δuxt2Δ* as above. Scale bars, 100 µm (top row) and 10 µm (bottom row). White arrows highlight fungi (stained turquoise). Images shown are representative of two independent studies (4-5 mice per group per experiment).

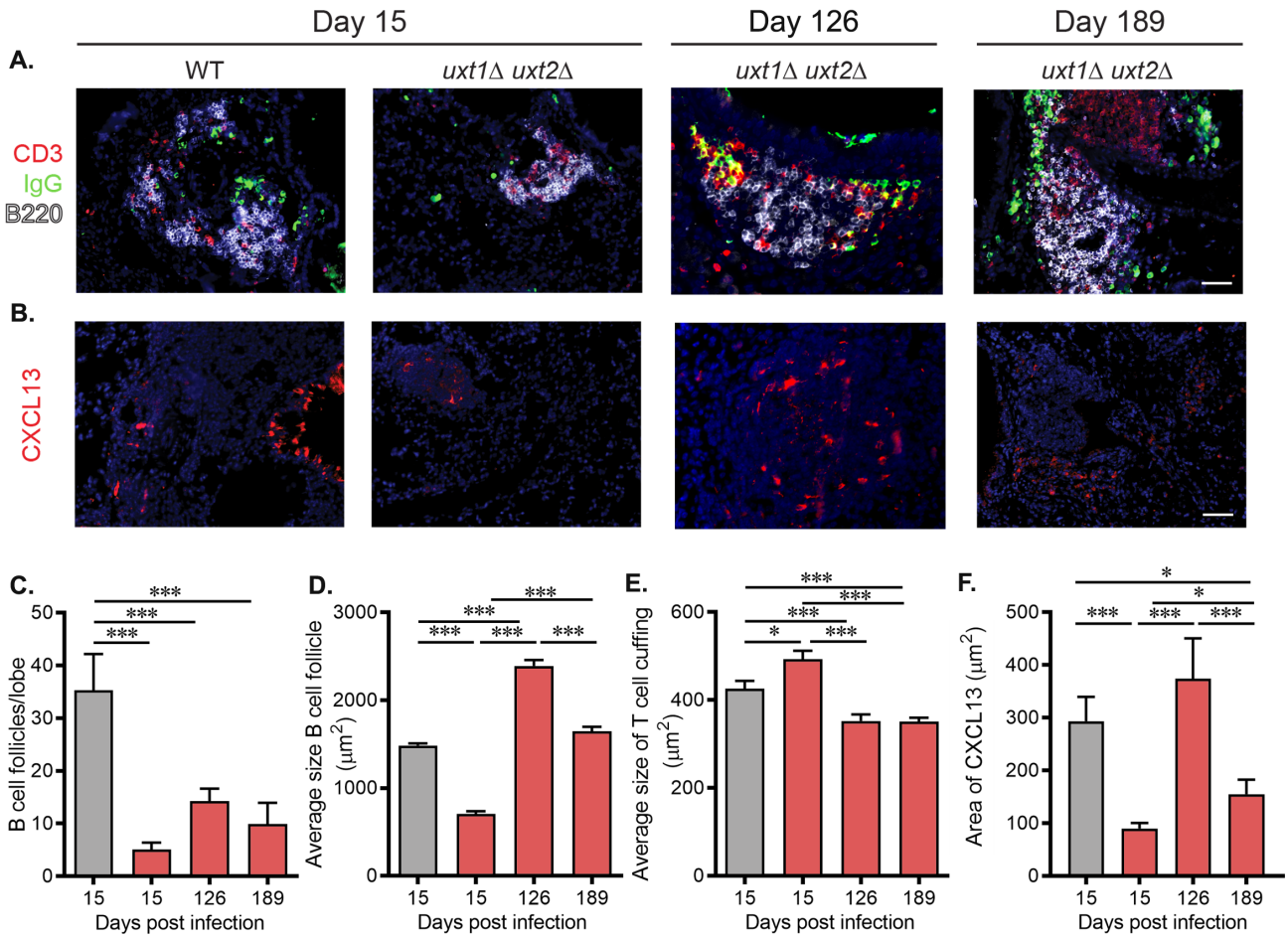

Figure 5. iBALT complexity in the context of *C. neoformans* infection. (A-B) Representative immunofluorescent staining of B cells ($B220^+$), T cells ($CD3^+$), plasma cells (IgG^+), and CXCL13 in the lungs of infected A/JCr mice. Scale bar = 100 μm. (C-E) Morphometric analysis of iBALT structures in A/JCr mice infected with WT (gray bars) and *uxt1*Δ *uxt2*Δ (red bars). (F) Quantification of immunofluorescent staining of CXCL13. Plots show the combined mean ± SEM of two independent studies (4-5 mice per group per experiment); colors as in panels C-E. *, $p < 0.05$; ***, $p < 0.005$ by Student's t-test.

SUPPLEMENTARY MATERIAL

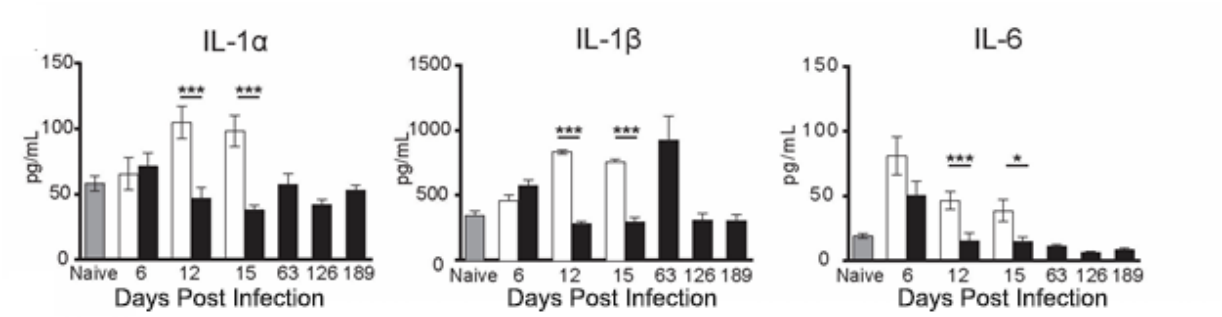

Supplemental Figure 1. Pro-inflammatory cytokines in lung homogenates at the indicated dpi (grey, naïve; white, WT; black, *uxt1*Δ *uxt2*Δ). Results shown are for individual mice from two independent experiments (n = 5 per group per experiment) and are plotted with the mean ± SEM. *, $p < 0.05$; **, $p < 0.01$; ***, $p < 0.005$ by Student's t-test.

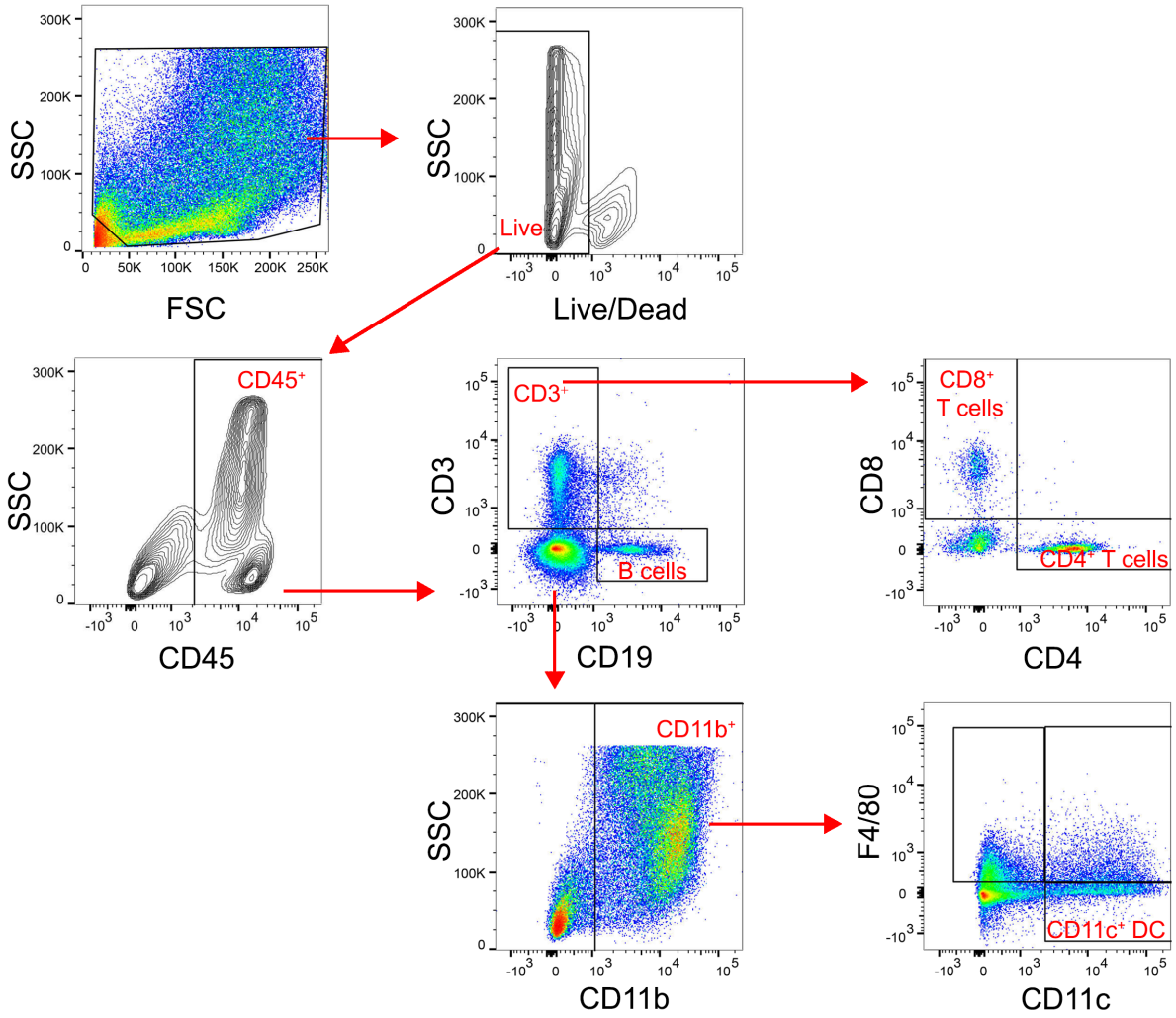

Supplemental Figure 2. Example of the multi-color flow cytometry gating strategy used to enumerate lung infiltrating immune cells.

Table S1. *C. neoformans* strains utilized in these studies.

C. neoformans strain[a]	Origin
KN99α	(Nielsen et al., 2003)
*uxt1*Δ	(Li et al., 2018)
UXT1	(Li et al., 2018)
*uxt2*Δ	(Li et al., 2018)
UXT2	(Li et al., 2018)
*uxt1*Δ *uxt2*Δ	(Li et al., 2018)
*uxs1*Δ	(Gish et al., 2016)
*cap59*Δ	(Moyrand and Janbon, 2004)

[a] All mutant strains are derived from KN99α

Table S2. Antibodies for flow analysis.

Antigen	Clone	Fluorophore	Dilution	Company
CD3	17-A2	APC-Cy7	1:250	BioLegend
CD4	GK1.5	BUV737	1:500	BD Biosciences
CD8a	53-6.7	BV650	1:125	BD Biosciences
CD11b	M1/70	BV510	1:250	BD Biosciences
CD11c	N418	PE	1:125	BD Biosciences
CD1/CD32 Fc Block	2.4G2	(not applicable)	1:500	BD Biosciences
CD19	1D3	BV786	1:125	BD Biosciences
CD45	30-F11	Pacific Blue	1:250	BioLegend
F4/80	BM8	APC	1:250	Thermo

REFERENCES FOR SUPPLEMENTAL MATERIAL

Gish, S.R., Maier, E.J., Haynes, B.C., Santiago-Tirado, F.H., Srikanta, D.L., Ma, C.Z., Li, L.X., Williams, M., Crouch, E.C., Khader, S.A.*, et al.* (2016). Computational analysis reveals a key regulator of Cryptococcal virulence and determinant of host response. mBio *7*, e00313-00316.

Li, L.X., Rautengarten, C., Heazlewood, J.L., and Doering, T.L. (2018). Xylose donor transport is critical for fungal virulence. PLoS Pathog *14*, e1006765.

Moyrand, F., and Janbon, G. (2004). *UGD1*, encoding the *Cryptococcus neoformans* UDP-glucose dehydrogenase, is essential for growth at 37 degrees C and for capsule biosynthesis. Eukaryot Cell *3*, 1601-1608.

Nielsen, K., Cox, G.M., Wang, P., Toffaletti, D.L., Perfect, J.R., and Heitman, J. (2003). Sexual cycle of *Cryptococcus neoformans var. grubii* and virulence of congenic a and alpha isolates. Infection and immunity *71*, 4831-4841.